Received: 28 June 2022 | Revised: 9 August 2023 | Accepted: 16 August 2023

DOI: 10.1002/asl.1189

RESEARCH ARTICLE

Atmospheric Science Letters RMetS

Boundary layer profile of decaying and non-decaying tropical storms near landfall

Enoch Yan Lok Tsui[1,2] | **Pak Wai Chan**[3] | **Ralf Toumi**[1,2]

[1]Department of Physics, Imperial College London, London, UK

[2]Leverhulme Centre for Wildfires, Environment and Society, London, UK

[3]Hong Kong Observatory, Tsim Sha Tsui, Kowloon, Hong Kong, China

Correspondence
Enoch Yan Lok Tsui, Department of Physics, Imperial College London, London, SW7 2AZ, UK.
Email: e.tsui20@imperial.ac.uk

Funding information
Leverhulme Trust, Grant/Award Number: RC-2018-023; Singapore Green Finance Centre; UK Research and Innovation, Grant/Award Number: UKRI-NE/V017756/1

Abstract

The vertical profile of the wind structure of translating tropical cyclones, including the associated azimuthal asymmetry, has been the subject of existing theoretical and observational studies using dropsondes. Most of these studies are based on data collected from relatively strong cyclones over the Atlantic. Here we explore the tropical cyclone boundary layer wind profile of mainly relatively weak landfalling cyclones near Hong Kong. We find that decaying tropical storms have a much larger mid- to low-level inflow angle than those that are intensifying or in steady-state. The inflow angles of intensifying, steady-state and decaying tropical storms converge towards the top of the boundary layer. The wind speed reduces through the boundary layer in a similar way in all three cases. The combination of these factors means that decaying tropical storms have stronger inflow than intensifying and steady-state ones. We attribute these local effects to remote enhanced surface friction over land when the storms are weakening.

KEYWORDS

boundary layer, inflow, landfall, tropical cyclone, tropical storm, wind profile, wind profiler

1 | INTRODUCTION

The vertical profile and azimuthal asymmetry of tropical cyclones in the boundary layer (BL) and above has been studied (e.g., Kepert, 2001; Kepert & Wang, 2001; Knupp et al., 2000; Ren et al., 2019; Shapiro, 1983; Thomsen et al., 2015). Zhang and Uhlhorn (2012) and Zhang et al. (2021) focused on the surface. Rogers et al. (2013), Liao et al. (2019) and He et al. (2022) studied the effects of cyclone intensity change while Powell (1982), Knupp et al. (2006) and Hlywiak and Nolan (2022) studied the effects of landfall. These studies, with the exception of Knupp et al. (2006), mostly involve relatively strong cyclones at or above Category 1 on the Saffir–Simpson hurricane wind scale (hereafter TC). Here, our objective is to identify for the first time any differences in the BL profiles of relatively weak systems with intensities at tropical storm (TS) level. We will explore if there are structural differences among intensifying, steady-state and decaying TS.

Shapiro (1983) observed stronger winds on the left of translating TCs with maximum inflow in the front-right quadrant. Ren et al. (2019) reported that the low-level radial velocity is larger in the front and the inflow layer depths in all four quadrants are well below 1500 m, ranging from below 500 m to slightly over 1000 m. Knupp et al. (2000) observed strong inflow below 1000 m for Hurricane Georges (1998) at landfall. Zhang and Uhlhorn (2012)

reported an average near-surface inflow angle between 18° and 30° with azimuthal asymmetry that grows in amplitude and shifts counterclockwise in phase as cyclone translation speed increases but not very sensitive to cyclone intensity. At low translation speeds, the largest (smallest) inflow angle is found in the rear-right (front-left).

Rogers et al. (2013) reported that intensifying TCs show stronger near-surface inflow and have deeper inflow layer compared with steady-state ones. This is consistent with Kepert (2001) that inertially less stable cyclones have larger depth scales. In the observations of Liao et al. (2019), intensifying cyclones are characterised by a BL either dominated by inflow or with inflow that strengthens towards the cyclone centre; while weakening cyclones by a BL dominated by outflow. On the other hand, He et al. (2022) observed weak inflow in the BL of the weakening TS Khanun (2017). The inflow angle is also important in controlling the size of cyclones (Wang & Toumi, 2022).

Powell (1982) observed from the landfalling Hurricane Frederic (1979) that landfall shifts the region of maximum inflow angle from the rear-right to the landward side due to increased surface friction over land. Knupp et al. (2006) studied TS Gabrielle (2001) during landfall and reported that changes in the BL wind profile occurred within 5 km of the upstream side of the coastline. Hlywiak and Nolan (2022) performed simulations of TCs making perpendicular landfall with a straight coastline. They found high inflow angle and weakening winds over land, and an enhanced and deepened inflow layer in the offshore flow. These are attributed to the difference in surface friction over land (high) and water (low). The described responses begin 6–9 h before landfall when the cyclone is about 200 km from land.

Here we provide a new perspective. We found that intensifying and steady-state TS have fairly similar BL wind profiles which are distinct from decaying TS closer to land. The decaying TS has stronger mid- to low-level inflow mainly driven by higher inflow angle under near identical reduction in wind speed from the top of the BL compared with intensifying and steady-state TS. We believe such differences in the behaviour of decaying TS from that of intensifying and steady-state TS arise from the effects of enhanced surface friction due to their proximity to land.

2 | DATA AND METHODS

2.1 | Data

The BL zonal (u-) and meridional (v-) wind velocities are provided by the Hong Kong Observatory (HKO) and were measured by the wind profiler fitted at the Sha Lo Wan weather station (113.9° E, 22.3° N) in the north of Lantau Island, Hong Kong. The wind profiler measures the wind velocity throughout the BL directly above with a vertical resolution of about 50 m at regular 10-min intervals. Detailed description on the working principle of the wind profiler can be found for example in Tse et al. (2013). Measurements at each altitude and each time step are quality controlled. Data from days with tropical cyclones near Hong Kong are available from 2010 to 2019. Due to a system replacement in Spring 2016, the measurement altitudes before and after are slightly shifted. To combine data from the two periods, we treated measurements at each actual measurement altitude as being measured at the nearest 50 m between 200 and 1400 m inclusive.

For each tropical cyclone in the HKO dataset, the radius of maximum wind speed ($R_{\max}$), 1-min maximum sustained wind speed ($V_{\max}$), coordinates of the cyclone centre and its distance to land at regular 6-h interval are taken from NOAA's IBTrACS Version 4 (Knapp et al., 2010, 2018). These are linearly interpolated to 10-min time steps to match with the HKO data. The translation speed (V_{trans}) and direction of the cyclones are further obtained from the interpolated coordinates. The interpolated coordinates are also used to compute the distance R between the cyclone centre and the weather station, which is then normalised by the interpolated $R_{\max}$ to give $r = R/R_{\max}$.

Kepert (2001) provided an analytical solution for the inner core of translating tropical cyclones under a linear model and showed that inertially less stable cyclones have larger depth scales. The linearisation requires the cyclone translation speed to be much smaller than the gradient level flow (hereafter K01 criterion). In the approach presented by Shapiro (1983), relatively slow translation of the cyclone is also necessary for the linearisation there to hold. The relative magnitude between cyclone translation speed and tangential wind speed is not a main point of concern if relatively strong cyclones are considered as the latter is always high. However, by focusing on relatively weak cyclones here, we only consider data taken when the K01 criterion is met as explained below.

In this study, we confine ourselves to those HKO data deemed valid by their internal quality control algorithm taken from landfalling ($r < 4$) cyclones reaching at least TS intensity ($V_{\max} \geq 34$kt) and meeting the K01 criterion at the time of measurement. The K01 criterion is deemed met if the wind speed at the top of the BL is at least four times the cyclone translation speed. Note that the condition we set for landfalling is rather strong—we consider the distance from the weather station but not the closest distance from land. This has the added benefit of

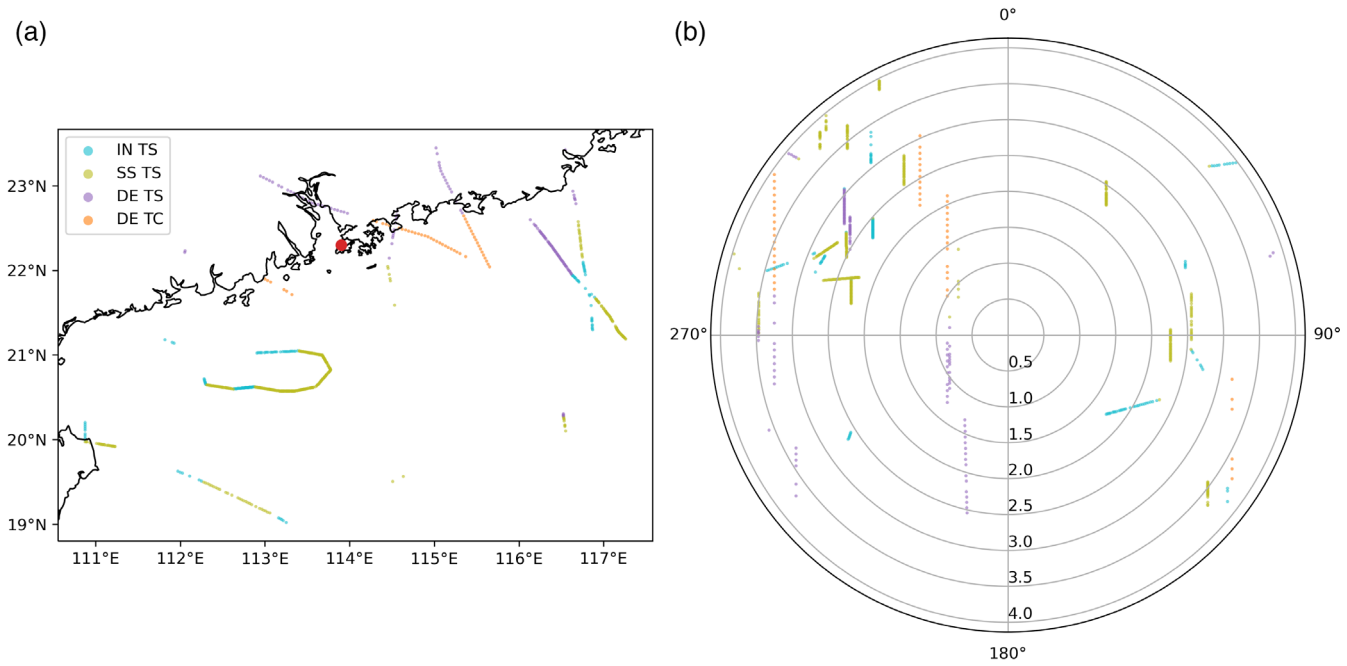

FIGURE 1 Spatial distribution of wind profiler samples, classified into intensifying (IN) TS, steady-state (SS) TS, decaying (DE) TS and DE TC. (a) Geographic location of cyclone centre at the time of measurement. Location of the Sha Lo Wan weather station is indicated by the red dot. (b) Azimuthal angle (relative to the direction of cyclone translation) and distance (normalised by R_{max}) of the Sha Lo Wan weather station from cyclone centre at the time of measurement.

TABLE 1 Intensifying TS measurements summary statistics.

			V_{max} (kt)			r			V_{trans} (ms^{-1})		
	n	**Cyclone**	**Min**	**Median**	**Max**	**Min**	**Median**	**Max**	**Min**	**Median**	**Max**
ALL	131	5	34	41	50	1.8	2.6	4.0	1.2	2.3	5.3
FR	**14**	**1**	**34**	**40**	**41**	**2.6**	**3.7**	**4.0**	**3.8**	**4.2**	**4.2**
RR	**37**	**3**	**34**	**42**	**45**	**1.8**	**2.0**	**3.8**	**2.5**	**2.5**	**5.3**
RL	7	1	34	34	35	2.6	2.6	2.7	1.9	1.9	1.9
FL	**73**	**3**	**35**	**40**	**50**	**2.3**	**2.7**	**3.5**	**1.2**	**1.6**	**2.7**

Note: Bold for quadrants with at least 10 samples.

TABLE 2 Steady-state TS measurements summary statistics.

			V_{max} (kt)			r			V_{trans} (ms^{-1})		
	n	**Cyclone**	**Min**	**Median**	**Max**	**Min**	**Median**	**Max**	**Min**	**Median**	**Max**
ALL	384	7	35	40	60	0.9	2.6	4.0	0.8	1.3	5.3
FR	**61**	**2**	**35**	**40**	**40**	**2.3**	**2.5**	**3.7**	**1.0**	**1.0**	**4.6**
RR	**56**	**2**	**35**	**40**	**40**	**2.3**	**2.3**	**3.7**	**1.3**	**1.7**	**5.3**
RL	0	0	–	–	–	–	–	–	–	–	–
FL	**267**	**6**	**35**	**40**	**60**	**0.9**	**2.7**	**4.0**	**0.8**	**1.3**	**4.6**

Note: Bold for quadrants with at least 10 samples.

ensuring that all measurements considered were made relatively close to the cyclone centre.

In total, 690 wind profiler measurements taken from 12 individual cyclones over the 10-year observation period entered into this study. Figure 1 shows the spatial distribution of cyclone centre at the times of measurement. Summary statistics of the corresponding cyclone properties are shown in Tables 1–4. The data are sorted

TABLE 3 Decaying TS measurements summary statistics.

			V_{max} (kt)			r			V_{trans} (ms^{-1})		
	n	**Cyclone**	**Min**	**Median**	**Max**	**Min**	**Median**	**Max**	**Min**	**Median**	**Max**
ALL	124	7	34	44	64	0.8	2.8	4.0	1.4	2.7	7.3
FR	2	1	34	34	34	3.8	3.8	3.9	2.9	2.9	2.9
RR	0	0	–	–	–	–	–	–	–	–	–
RL	**53**	**4**	**38**	**58**	**63**	**0.8**	**1.7**	**3.7**	**2.6**	**6.9**	**7.3**
FL	**69**	**5**	**35**	**42**	**64**	**0.8**	**2.8**	**4.0**	**1.4**	**2.2**	**7.3**

Note: Bold for quadrants with at least 10 samples.

TABLE 4 Decaying TC measurements summary statistics.

			V_{max} (kt)			r			V_{trans} (ms^{-1})		
	n	**Cyclone**	**Min**	**Median**	**Max**	**Min**	**Median**	**Max**	**Min**	**Median**	**Max**
ALL	51	3	64	69	114	1.0	2.9	3.9	6.4	6.9	7.3
FR	0	0	–	–	–	–	–	–	–	–	–
RR	6	1	106	110	114	3.2	3.4	3.7	6.4	6.4	6.4
RL	0	0	–	–	–	–	–	–	–	–	–
FL	**45**	**2**	**64**	**68**	**74**	**1.0**	**2.7**	**3.9**	**6.7**	**6.9**	**7.3**

Note: Bold for quadrants with at least 10 samples.

into quadrants and classified by intensity and intensification rate as explained in Section 2.2. Notice that the intensifying and steady-state cyclones are located further away from land while the decaying cyclones are considerably closer to or even over land when measurements were taken. In addition, the measurements are biased in terms of azimuthal angle relative to cyclone translation direction, with the majority having been taken in the front-left.

2.2 | Methods

All BL profiles are considered in a frame of reference translating with the cyclone and are obtained from the wind velocities $(\widetilde{u},\widetilde{v})$ after subtracting the cyclone translation velocity from the wind velocities (u,v) measured by the wind profiler. For each measured wind profile, at a certain altitude the full wind speed is the magnitude of the wind velocity at that altitude while the radial velocity is the component along the direction pointing from the cyclone centre to the weather station (negative for inflow). The inflow angle α at altitude h is computed using

$$\alpha(h) = -\text{atan2}[\widetilde{v}(h),\widetilde{u}(h)] - \Phi, \tag{1}$$

mapped onto $(-180^\circ, 180^\circ]$, where Φ is the compass bearing from the weather station to the cyclone centre. This gives the angle of deviation of the wind from the tangential direction relative to the cyclone centre (negative for anticlockwise deviation, i.e., inflow in the Northern Hemisphere). The reduction factor ξ at altitude h is computed with respect to a reference altitude h_{ref} according to

$$\xi(h) = \sqrt{\frac{[\widetilde{u}(h)]^2 + [\widetilde{v}(h)]^2}{[\widetilde{u}(h_{ref})]^2 + [\widetilde{v}(h_{ref})]^2}}. \tag{2}$$

It describes the ratio by which the wind speed has reduced between h_{ref} and h. A proper h_{ref} should be set high enough so that all measured wind profiles are near geostrophic at h_{ref}. If this is the case, ξ should be near constant around h_{ref}. Throughout this study, we set $h_{ref} = 1250\,\text{m}$, which is justified retrospectively. We also implicitly consider the chosen h_{ref} to be representative of the BL height, which is reasonable (Ren et al., 2019).

The processed BL profiles are grouped by whether at the time of measurement the cyclone was weak (TS intensity, $34\,\text{kt} \le V_{max} < 64\,\text{kt}$) or strong (TC intensity, $V_{max} \ge 64\,\text{kt}$) and whether the cyclone was intensifying, in steady-state or decaying. Following Rogers et al. (2013), the cyclone is deemed intensifying (decaying) if V_{max} is increasing (decreasing) faster than $20\,\text{kt}\,\text{day}^{-1}$ and in steady-state if V_{max} is changing at a rate between $\pm 10\,\text{kt}\,\text{day}^{-1}$. The individual BL profiles of the same variable are then composited by averaging. To account for

the azimuthal asymmetry of translating cyclones and the directional bias in sampling, both full-sample average and individual quadrant averages are considered. For full-sample average, at each altitude the arithmetic mean with equal weight is taken across all individual profiles with available data. For individual quadrant averages, the arithmetic means are computed similarly but separately for profiles measured with the weather station, respectively, located in the front-right, rear-right, rear-left and front-left of the cyclone relative to translation direction. Throughout this study, data points averaged from less than 10 individual BL profiles are discarded.

The analysis is repeated on just the profiles from TS sorted by distance to land.

3 | RESULTS

We computed the inflow angle, reduction factor and radial velocity BL profiles from the HKO wind profiler measurements. Based on the data available, we only compared the full-sample and front-left quadrant averages of intensifying TS, steady-state TS, decaying TS and decaying TC. While the full-sample averages generally agree with the front-left quadrant averages, due to the azimuthal asymmetry and sampling bias, the front-left quadrant averages should be more reliable quantitatively.

As can be seen from Figure 2, the BL inflow angle profiles of intensifying and steady-state TS are fairly similar while that of decaying TS stands out. The full-sample average (Figure 2a) suggests that the inflow angle of decaying TS at 200 m is nearly double that of intensifying and steady-state TS. This approximate doubling of inflow angle at low-level is confirmed by the front-left quadrant analysis (Figure 2b). There, we see that the inflow angle of intensifying TS remains fairly constant at around 20° throughout much of the BL. It increases to around 30° as altitude descends from 600 m to 200 m. The inflow angle of steady-state TS is around 28° towards the top of the BL. Descending into the BL, it decreases to converge with intensifying TS at around 1100 m and remains close to intensifying TS down to around 600 m. It then increases more steeply than intensifying TS to around 46° as altitude further descends to 200 m. As for decaying TS, its inflow angle is similar to those of intensifying and steady-state TS towards the top of the BL and increases throughout the BL to around 80° as altitude descends to 200 m. Despite the lack of data nearer the surface, it seems likely that decaying TS will also have a much larger near-surface inflow angle than intensifying and steady-state TS.

Despite marked differences in the BL inflow angle profile of decaying TS from intensifying and steady-state TS, Figure S1a shows similar BL reduction factor profile for all intensifying, steady-state and decaying TS. The

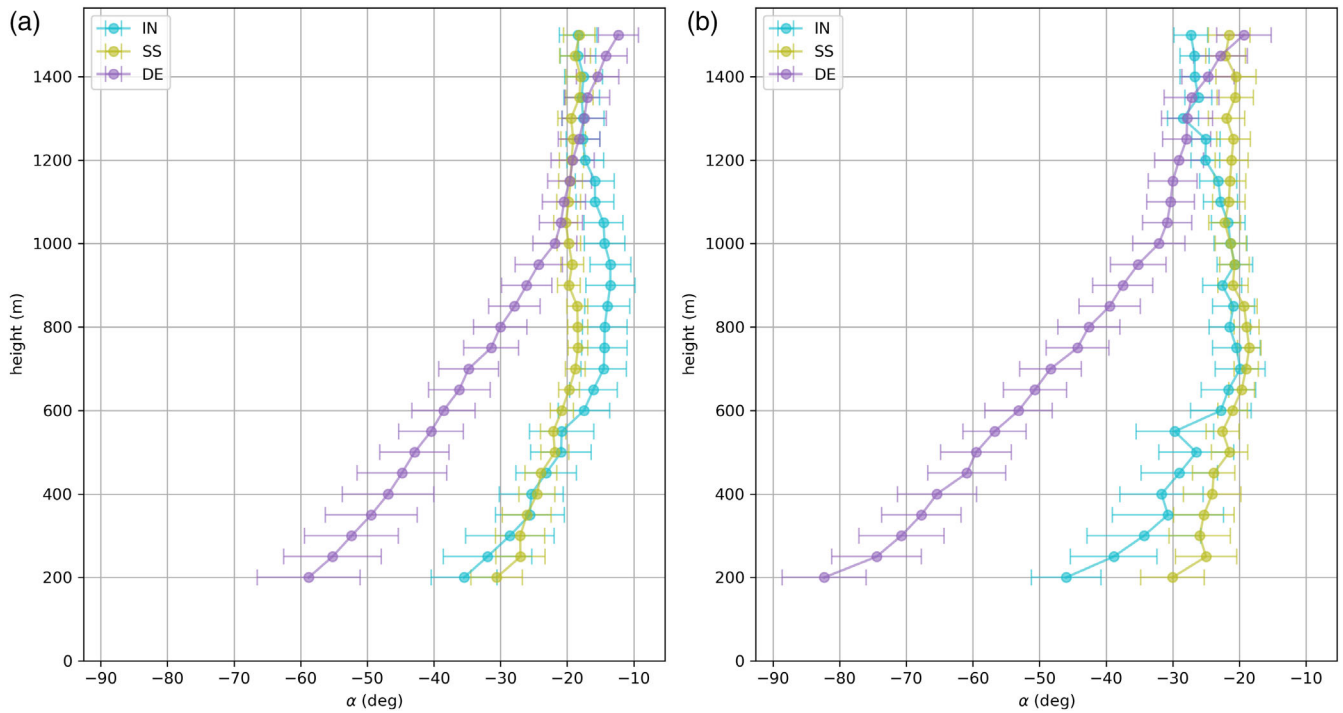

FIGURE 2 Boundary layer profile of inflow angle for intensifying (IN), steady-state (SS) and decaying (DE) TS averaged over (a) all samples and (b) samples in the front-left quadrant.

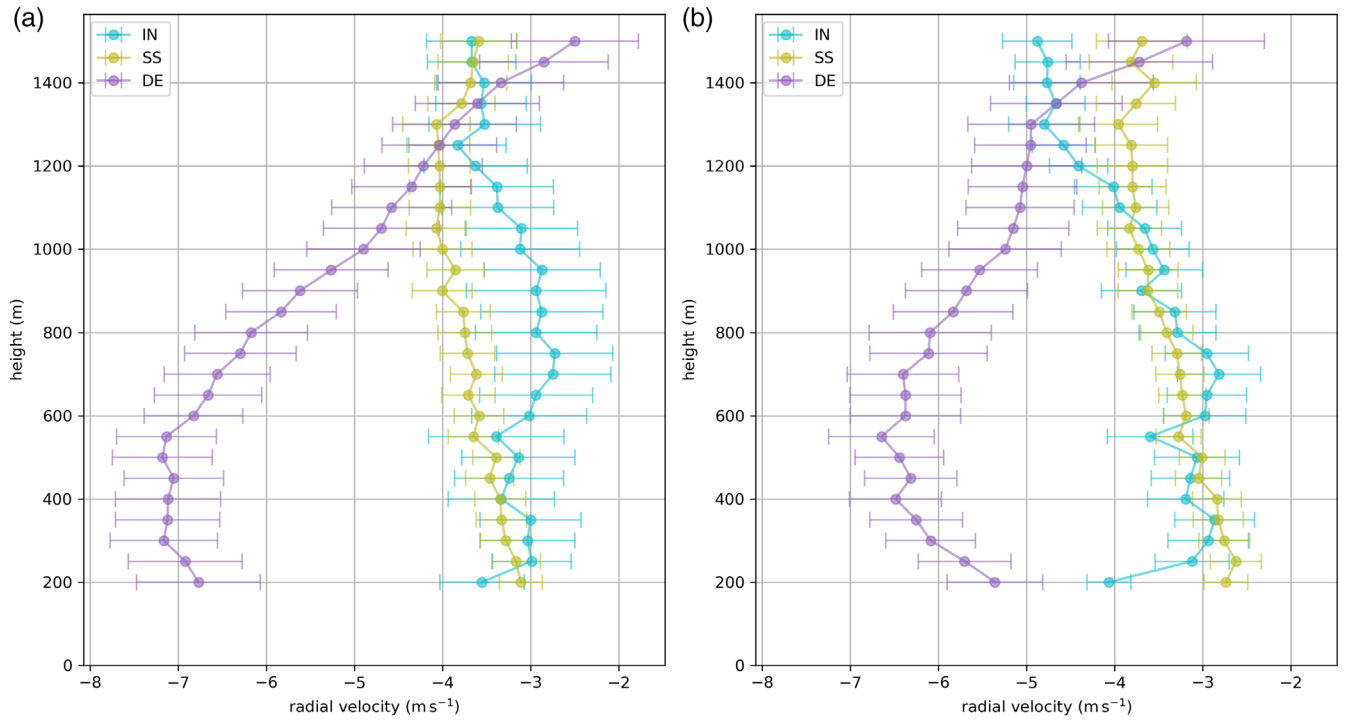

FIGURE 3 Same as Figure 2 but for radial velocity.

similarity is even more striking if we focus on the front-left quadrant (Figure S1b). Staying at around unity above the reference altitude of 1250 m, the reduction factor decreases at a fairly constant rate below to around 0.55 as altitude descends to 200 m.

Figure 3 shows the BL radial velocity profiles of intensifying, steady-state and decaying TS. As would be expected based on the inflow angle and reduction factor profiles (Figures 2 and S1), the radial velocity profiles of intensifying and steady-state TS are fairly similar while that of decaying TS stands out. The radial velocities of intensifying, steady-state and decaying TS appear to have similar values, especially taking uncertainties into account, towards the top of the BL. Those of intensifying and steady-state TS generally decrease throughout the BL as altitude descends to 200 m. Over the same altitude range, the radial velocity of decaying TS tends to increase, showing sign of recurve at low-levels. In the mid- to low-level, the radial velocity of decaying TS is clearly larger than those of intensifying and steady-state TS. This means decaying TS has a stronger inflow layer than intensifying and steady-state TS.

Sorting the TS BL profiles by the centre's distance to land produces results that resemble the above. This is robust across different threshold distances from 50 to 140 km, where a threshold of 80 km (Figures S2–S4) gives the closest match in behaviour between the close to (far from) land group and the decaying (intensifying and steady-state) group. However, this is neither surprising nor very helpful as, for example, with 80 km threshold, around 71.2% (93.6%) of the front-left quadrant profiles in the close to (far from) land group are also from decaying (intensifying and steady-state) TS. A comparison between Figures 1 and S5 also illustrates this point.

Looking at decaying TS and TC, we see that all basic features in the BL profiles are common across the two, differing only in size and scale. Decaying TC has smaller inflow angle than decaying TS throughout the BL (Figure S6). Descending through the BL, the reduction in wind speed in decaying TC is weaker than in decaying TS (Figure S7). Finally, decaying TC has stronger inflow than decaying TS throughout the BL with a peak in radial velocity lower in altitude (Figure S8).

4 | DISCUSSION

We analysed 12 storms making landfall near Hong Kong and observed for the first time that there is a difference in the BL inflow angle profiles between decaying and non-decaying (intensifying and steady-state) TS. Starting with similar value at the top of the BL, the inflow angle of decaying TS increases steadily as altitude descends through the BL while that of non-decaying TS only starts to increase pass 600 m, reaching only about half that of decaying TS at 200 m. Meanwhile, the reduction factors of decaying and non-decaying TS are similar throughout the BL. These combine to give a stronger inflow layer in

decaying TS than in non-decaying TS. This result can be reproduced by separating the profiles by the TS centre's distance to land, where the close to (far from) land group matches with the decaying (non-decaying) group. Comparing decaying TS and TC, we see that all basic features in the BL profiles are common across the two, differing only in size and scale.

Unlike Knupp et al. (2006) with landfalling TS Gabriel (2001), we do not observe the presence of jets from any of our composite TS BL profiles. The absence of jets from TC near Hong Kong based on HKO data has previously been reported by Tse et al. (2013). The decaying TC BL radial velocity profile we observed (Figure S8) appears to agree with Ren et al. (2019) that the inflow layer of a TC is well below 1500 m. It is also compatible with that observed by Knupp et al. (2000) from landfalling Hurricane Georges (1998) and with the simulation results by Hlywiak and Nolan (2022) and Kepert and Wang (2001).

Although Rogers et al. (2013) observed stronger near-surface inflow and deeper inflow layer in intensifying TCs compared with steady-state ones, citing larger depth scales for inertially less stable cyclones (Kepert, 2001), we do not see such differences in our TS observations. Furthermore, unlike Liao et al. (2019), there is no sign of outflow in the BL of our decaying TS or TC. Our observations show that intensifying and steady-state TS have similar inflow throughout the mid- to low-level of the BL while that of decaying TS is clearly stronger (Figure 3). Meanwhile, the individual BL wind profiles of intensifying, steady-state and decaying TS, especially for the front-left quadrant, were taken from TS with similar $V_{\max}$ (Tables 1–3), hence largely similar inertial stability.

Sparks and Toumi (2022a) showed how surface pressure increases are driven by the net inflow into the column for a weakening storm. The pressure tendency depends on both the inflow and the size of the cyclone (Sparks & Toumi, 2022b). Their framework does not invoke inertial stability and is consistent with the observations here. We hypothesise that the difference in inflow strength between our decaying and non-decaying TS is not due to inertial stability of the cyclones but their proximity to land (Figure 1a).

Measurements of decaying cyclones were taken when their centres were considerably closer to or even over land. This is not the case for non-decaying cyclones. We also compared the BL profiles based on the TS centre's distance to land and found that the behaviour of the close to (far from) land group matches with the decaying (non-decaying) group. However, given the large overlap of profiles across these two classifications, this cannot be considered a robust independent result.

The effect of inertial stability of the cyclone can be assessed by comparing our decaying TS (weaker) and TC (stronger). Decaying TC are inertially more stable due to their higher wind speeds. Nevertheless, they have similar but scaled BL profiles compared with decaying TS. The way in which the BL profiles, described by the reduction factor (Figure S7) and radial velocity (Figure S8), scale between the two appear to agree with Kepert (2001) that inertially less stable cyclones have larger depth scales. However, while the BL profiles of decaying TS and TC are similar, non-decaying TS behave differently.

The stronger inflow in the mid- to low-level of the BL in our decaying TS compared with non-decaying TS is driven by larger inflow angle throughout the BL under similar wind reduction (normalised wind speed profile). It is then important to understand how enhanced surface friction due to land can modify the inflow angle without affecting the normalised wind speed profile. The eddy diffusivity (ED), through its effect on the production of turbulence kinetic energy, plays a central role in governing the shape of the wind speed profile and the BL height. Surface friction affects the atmosphere by causing mesoscopic turbulence and modifying the ED near the surface. However, above this surface layer, atmospheric properties such as the shear and stability rather than surface roughness are dominant in determining the ED. In other words, the primary effect of surface friction on the atmosphere is in modulating its surface layer thickness. Grisogono (2011) showed that for a BL with altitude-dependent ED, both the near-surface wind deflection angle and BL height can depend on such parameters as the overall strength of the ED and the surface layer thickness. It was shown for the ED profile $K(z) = K_0(z/h)\exp\left[-0.5(z/h)^2\right]$ that when $K_0 > 1\,\mathrm{m^2\,s^{-1}}$, the near-surface wind deflection angle is sensitive to changes in both the surface layer thickness and K_0. However, the BL height is only weakly sensitive to such changes. Changing the surface friction can lead to a different inflow angle while maintaining similar normalised wind speed profile shape in the BL. Therefore, enhanced surface friction due to land is a plausible explanation to our observed differences in the BL of decaying and non-decaying TS.

Previous studies used data collected from fairly evenly spatially distributed dropsondes. The distance of the cyclone centre from land at measurement, the distance of measurement from the cyclone centre, and the azimuthal angle of measurement relative to cyclone translation direction can all be controlled to eliminate bias in sampling. In contrast, our use of a ground-based instrument at a fixed weather station means that the three parameters just mentioned are not independent for the samples in our dataset. The most significant drawbacks are that

there is inevitable bias in sampling rate through the azimuthal angle of measurement relative to cyclone translation direction and that certain quadrants will have a markedly higher proportion of data taken post-landfall. As a result, simply taking the sample mean is inappropriate due to azimuthal asymmetry in translating tropical cyclones. We tried to overcome this bias by analysing the four quadrants relative to cyclone translation direction separately. However, we have enough data to study the front-left quadrant only. The deficiency in data hindered our attempt to study the azimuthal asymmetry in TS near landfall and the effect of the flow being onshore or offshore. Finally, the lack of non-decaying (decaying) TS close to (far from) land in our dataset means that results from sorting the TSs by their centre's distance to land should not be taken as an independent piece of evidence to support our hypothesis.

5 | CONCLUSION

The BL wind profiles measured within $4R_{max}$ from 12 tropical cyclones making landfall near Hong Kong were analysed. These profiles were acquired with a wind profiler between 2010 and 2019 at the Sha Lo Wan weather station in Hong Kong. These measurements revealed that the inflow angles of intensifying and steady-state TS are similar to each other throughout the BL but smaller than those of decaying TS, especially in the mid- to low-level of the BL. Converging towards the top of the BL, the inflow angle of decaying TS is roughly double that of intensifying and steady-state TS at an altitude of 200 m. On the other hand, the wind speed reduces through the BL in a similar way in all three cases. The stronger inflow in decaying TS compared with intensifying and steady-state ones is then mainly driven by the larger inflow angle of decaying TS throughout the BL. Inertial stability has been put forward to explain the differences in BL profile between stronger cyclones that are intensifying and in steady-state (e.g., Rogers et al., 2013). Here, we instead observed differences between decaying and non-decaying TS and argued that the effects of enhanced friction by land due to proximity in the decaying TS is the likely main driver of the differences observed here. In general, the flow being onshore or offshore could also have an effect. This however could not be and was not assessed here limited by the HKO dataset. These effects should also apply to other coastal locations.

AUTHOR CONTRIBUTIONS

Enoch Yan Lok Tsui: Conceptualization; data curation; formal analysis; investigation; methodology; software; validation; visualization; writing – original draft; writing – review and editing. **Pak Wai Chan:** Data curation; writing – review and editing. **Ralf Toumi:** Conceptualization; formal analysis; funding acquisition; investigation; methodology; project administration; resources; supervision; validation; writing – review and editing.

ACKNOWLEDGEMENTS

This research was funded by the Leverhulme Centre for Wildfires, Environment and Society through the Leverhulme Trust, grant number RC-2018-023; the Centre for Greening Finance and Investment (UKRI), grant number UKRI-NE/V017756/1; and the Singapore Green Finance Centre. The authors would like to thank the Hong Kong Observatory for providing data measured by the wind profiler at their Sha Lo Wan station.

CONFLICT OF INTEREST STATEMENT

The authors declare no conflict of interests.

ORCID

Enoch Yan Lok Tsui https://orcid.org/0000-0003-1621-0443

Pak Wai Chan https://orcid.org/0000-0003-2289-0609

REFERENCES

Grisogono, B. (2011) The angle of the near-surface wind-turning in weakly stable boundary layers. *Quarterly Journal of the Royal Meteorological Society*, 137(656), 700–708.

He, J., Hon, K.K., Chan, P.W. & Li, Q.S. (2022) Dropsonde observations and numerical simulations of intensifying/weakening tropical cyclones over the northern South China Sea. *Weather*, 77(9), 332–338.

Hlywiak, J. & Nolan, D.S. (2022) The evolution of asymmetries in the tropical cyclone boundary layer wind field during landfall. *Monthly Weather Review*, 150(3), 529–549.

Kepert, J. (2001) The dynamics of boundary layer jets within the tropical cyclone core. Part I: linear theory. *Journal of the Atmospheric Sciences*, 58(17), 2469–2484.

Kepert, J. & Wang, Y. (2001) The dynamics of boundary layer jets within the tropical cyclone core. Part II: nonlinear enhancement. *Journal of the Atmospheric Sciences*, 58(17), 2485–2501.

Knapp, K.R., Diamond, H.J., Kossin, J.P., Kruk, M.C. & Schreck, C.J. (2018) *International best track archive for climate stewardship (IBTrACS) project, version 4*. West Pacific: NOAA National Centers for Environmental Information.

Knapp, K.R., Kruk, M.C., Levinson, D.H., Diamond, J.H. & Neumann, J.C. (2010) The international best track archive for climate stewardship (IBTrACS) unifying tropical cyclone data. *Bulletin of the American Meteorological Society*, 91(3), 363–376.

Knupp, K.R., Walters, J. & Biggerstaff, M. (2006) Doppler profiler and radar observations of boundary layer variability during the landfall of tropical storm Gabrielle. *Journal of the Atmospheric Sciences*, 63(1), 234–251.

Knupp, K.R., Walters, J. & McCaul, E.W. (2000) Doppler profiler observations of hurricane Georges at landfall. *Geophysical Research Letters*, 27(20), 3361–3364.

Liao, F., Su, R., Chan, P.W., Qi, Y. & Hon, K.K. (2019) Observational study on the characteristics of the boundary layer during changes in the intensity of tropical cyclones landing in Guangdong, China. *Advances in Meteorology*, 2019, 8072914.

Powell, M.D. (1982) The transition of the hurricane Frederic boundary-layer wind field from the open Gulf of Mexico to landfall. *Monthly Weather Review*, 110(12), 1912–1932.

Ren, Y., Zhang, J.A., Guimond, S.R. & Wang, X. (2019) Hurricane boundary layer height relative to storm motion from GPS dropsonde composites. *Atmosphere*, 10(6), 339.

Rogers, R., Reasor, P. & Lorsolo, S. (2013) Airborne doppler observations of the inner-core structural differences between intensifying and steady-state tropical cyclones. *Monthly Weather Review*, 141(9), 2970–2991.

Shapiro, L.J. (1983) The asymmetric boundary layer flow under a translating hurricane. *Journal of the Atmospheric Sciences*, 40(8), 1984–1998.

Sparks, N. & Toumi, R. (2022a) A physical model of tropical cyclone central pressure filling at landfall. *Journal of the Atmospheric Sciences*, 79(10), 2585–2599.

Sparks, N. & Toumi, R. (2022b) The dependence of tropical cyclone pressure tendency on size. *Geophysical Research Letters*, 49(19), e2022GL098926.

Thomsen, G.L., Smith, R.K. & Montgomery, M.T. (2015) Tropical cyclone flow asymmetries induced by a uniform flow revisited. *Journal of Advances in Modeling Earth Systems*, 7(3), 1265–1284.

Tse, K.T., Li, S.W., Chan, P.W., Mok, H.Y. & Weerasuriya, A.U. (2013) Wind profile observations in tropical cyclone events using wind-profilers and doppler SODARs. *Journal of Wind Engineering and Industrial Aerodynamics*, 115, 93–103.

Wang, S. & Toumi, R. (2022) An analytic model of the tropical cyclone outer size. *npj Climate and Atmospheric Science*, 5(1), 46.

Zhang, G., Li, X., Perrie, W. & Zhang, J.A. (2021) Tropical cyclone winds and inflow angle asymmetry from SAR imagery. *Geophysical Research Letters*, 48(20), e2021GL095699.

Zhang, J.A. & Uhlhorn, E.W. (2012) Hurricane sea surface inflow angle and an observation-based parametric model. *Monthly Weather Review*, 140(11), 3587–3605.

SUPPORTING INFORMATION

Additional supporting information can be found online in the Supporting Information section at the end of this article.

How to cite this article: Tsui, E. Y. L., Chan, P. W., & Toumi, R. (2023). Boundary layer profile of decaying and non-decaying tropical storms near landfall. *Atmospheric Science Letters*, e1189. https://doi.org/10.1002/asl.1189